Comparative Evaluation of Electrical Resistance Tomography, Positron Emission Particle Tracking and High-Speed Imaging for Analysing Horizontal Particle-Liquid Flow in a Pipe

Savari, Chiya; Li, Kun; Barigou, Mostafa

DOI:
10.1016/j.powtec.2024.119606

Document Version
Publisher's PDF, also known as Version of record

Citation for published version (Harvard):
Savari, C, Li, K & Barigou, M 2024, 'Comparative Evaluation of Electrical Resistance Tomography, Positron Emission Particle Tracking and High-Speed Imaging for Analysing Horizontal Particle-Liquid Flow in a Pipe', *Powder Technology*, vol. 438, 119606. https://doi.org/10.1016/j.powtec.2024.119606

Powder Technology 438 (2024) 119606

Contents lists available at ScienceDirect

Powder Technology

journal homepage: www.journals.elsevier.com/powder-technology

Comparative evaluation of electrical resistance tomography, positron emission particle tracking and high-speed imaging for analysing horizontal particle-liquid flow in a pipe

Chiya Savari, Kun Li [1], Mostafa Barigou [*]

School of Chemical Engineering, University of Birmingham, Edgbaston, Birmingham B15 2TT, UK

HIGHLIGHTS

- Study tackles particle-laden flows and development/selection of imaging techniques.
- ERT, PEPT and HSI are evaluated for particle-liquid pipe flow imaging and analysis.
- Newly developed ERT methodology estimates local particle velocity field effectively.
- Enhanced HSI emerges as a cost-effective method compared to PEPT and ERT.
- Combining PEPT for particle velocity and ERT for concentration gives best results.

GRAPHICAL ABSTRACT

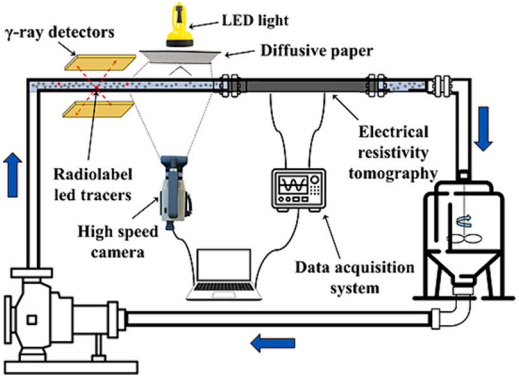

ARTICLE INFO

Keywords:
Pipe flow
Particle-liquid
PEPT
ERT
High-speed imaging
Two-phase flow field

ABSTRACT

We evaluate three experimental techniques - electrical resistance tomography (ERT), positron emission particle tracking (PEPT) and high-speed imaging (HSI) – for analysing the local particle velocity field and spatial distribution in a horizontal particle-liquid pipe flow under varying conditions of solid concentration. A new ERT methodology is devised for estimating particle velocity, circumventing the limitations of the conventional cross-correlation technique. Furthermore, an enhanced HSI approach is introduced and systematically compared with PEPT and ERT. Results show that, under all conditions, PEPT provides the most accurate particle velocity field followed by HSI, whilst ERT yields the most accurate concentration field, followed by HSI. The enhanced HSI emerges as a simple cost-effective option compared to PEPT and ERT. A combined measurement approach using PEPT for local particle velocity and ERT for local concentration, however, delivers the best comprehensive two-phase flow characterization, highlighting potential synergies between these methods for complex flow studies.

* Corresponding author.
E-mail address: m.barigou@bham.ac.uk (M. Barigou).
[1] KL is now at Shanxi Key Laboratory of Signal Capturing and Processing, North University of China, Taiyuan, 030051, China.

https://doi.org/10.1016/j.powtec.2024.119606
Received 21 December 2023; Received in revised form 28 February 2024; Accepted 6 March 2024
Available online 11 March 2024

1. Introduction

Turbulent particle-liquid pipe flow in horizontal pipes plays a pivotal role in industry, covering a wide range of important applications and posing unique design and operational challenges. In the process industries, this flow system is essential for transporting a variety of particulate materials, such as foods, pharmaceuticals, catalysts, minerals, slurries and solid reagents, within a variety of liquid carriers. The efficiency and effectiveness of these operations depend on precise control of particle dispersion, settling, and segregation [1,2]. Designing and operating pipelines that can accommodate varying particle sizes, densities and concentrations, whilst minimizing clogging and abrasion, is a significant challenge. Rational engineering solutions are essential to ensure consistent product quality and process efficiency, underscoring the importance of understanding and optimizing such particle-liquid flows. A range of experimental techniques have been developed to investigate particle-liquid flows, but a number of major challenges still exist, including: (i) obtaining accurate and representative data can be difficult due to the inherent complexities and dynamic nature of the flow; (ii) the wide range of liquid rheologies and particle properties such as size, shape, and density encountered in practice make reproducible accurate measurements often hard to obtain; (iii) particle transport under conditions of process intensification with enhanced solid concentrations poses additional difficulties; (iv) the opacity of such flows makes optical visualisation impossible; and (v) scale-up/scale-down of laboratory findings to real-world industrial conditions often faces monumental challenges. Therefore, further developments in flow diagnostic methods are needed to help improve our understanding of such flows and to help develop improved strategies for their industrial design, control and optimization.

Electrical resistance tomography (ERT) stands out as a prominent modality in process tomography, having undergone substantial advancements since its inception in the 1980s. The advantages of ERT lie in its multifaceted benefits, including high-speed capability, cost-effectiveness, absence of radiation hazards and non-intrusiveness. These attributes make ERT a promising technique for monitoring diverse industrial flows. ERT not only provides conductivity images but also facilitates the measurement of solid phase distribution and identification of flow regimes, as demonstrated by Lucas, et al. [3] and *Ma*, et al. [4]. Numerous studies have used ERT to analyse various flow scenarios, including Loh, et al. [5] and Lucas, et al. [3] who utilized ERT to monitor two-phase flows involving a non-conductive solid and a conductive liquid in both vertical and inclined pipes, and Wang, et al. [6] who explored ERT's efficacy in studying the velocity distribution and air volume fraction of gas–liquid swirling flows. Subsequently, ERT was successfully used to characterise the flow in liquid-solid as well as gas–liquid–solid circulating fluidized beds [7,8].

Whilst many works have successfully measured the solid phase distribution, accurate ERT measurement of local particle velocity particularly in solid-liquid flows remains a challenge. The conventional cross-correlation method applied in a dual-plane ERT system serves as the fundamental approach for assessing material velocity [3]. The transit time generally aligns with the moment when the cross-correlation function reaches its peak, reflecting signals that depict alterations in material distribution within a specific pixel of both the first and second planes of the tomographic unit. To facilitate effective flow analysis by this approach, it is imperative that a discernible pulse change in the conductivity of the mixture is induced, a necessity arising from the cross-correlation methodology, wherein the conductivity of corresponding pixels in the two planes is multiplied with various time delays. If the flow fails to exhibit such a peak, the classical cross-correlation method is incapable of accurately estimating velocity. However, even in the presence of a discernible peak, substantial errors in velocity estimation may occur when dealing with strongly noised input signals. Flows of mono-sized suspensions are particularly challenging since they exhibit a consistent particle distribution along the length of the pipe, and determination of the particle velocity field by cross-correlation is not possible.

Positron Emission Particle Tracking (PEPT) is a unique powerful technique that can be used to non-invasively probe particle-liquid flows. In PEPT, a positron-emitting radioactive particle tracer is injected in the flow and tracked in three-dimensional (3D) space and time. The annihilation of a positron with an electron, called an event, produces two back-to-back gamma rays. The detection of many such events by gamma-ray detectors positioned around the flow, enables via triangulation the 3D motion of the tracer to be tracked with remarkable accuracy and precision [9]. PEPT is ideally suited for the study of multiphase flows, allowing each component of the flow to be labelled and separately tracked to determine its long-term trajectory. The nature of each phase to be tracked in the flow will dictate the type of appropriate tracer to be used. PEPT offers a distinct and substantial advantage over leading optical techniques such as particle image velocimetry (PIV) and laser Doppler velocimetry (LDV), being able to image opaque flows and within opaque apparatus with matching accuracy [10]. PEPT has been extensively used in different particle-liquid flow systems [9,11–16]. Notwithstanding the merits associated with PEPT, its widespread adoption has been impeded by its high capital and operational cost, inherent radiation hazards and limited global availability. Furthermore, whilst the local occupancy data of the radiolabelled tracer, have facilitated the accurate estimation of solid phase distributions in laminar and turbulent pipe flows of nearly-neutrally buoyant particles based on the assumption of flow ergodicity [17,18], this methodology may not be applicable to the pipe flow of denser particles wherein ergodicity is questionable.

Amongst the laser-based methods most commonly used to visualize particle-liquid flows are PIV and LDV [19–23]. However, because of their dependence on light transmission, these optical techniques are limited to very dilute mixtures which are generally of little industrial relevance. Recent advancements in high-speed camera technology have yielded enhanced capabilities for faster image sampling, higher resolution and reduced costs, making high-speed imaging (HSI) coupled with sophisticated image analysis a viable alternative for determining particle velocities and particle distributions even in concentrated flows. High-speed digital cameras accompanied by advanced image processing algorithms have been applied in a number of multiphase flow scenarios, including solid-liquid, gas-liquid and gas-solid systems [24–28]. Despite these applications, the potential of this promising technique remains untapped in the examination of local particle velocities and spatial particle distribution in particle-liquid pipe flows with coarse particles and high concentrations. With further enhancement, HSI has the potential to yield valuable insights into the detailed local dynamics of particle-liquid flows in the form of Lagrangian particle trajectories which would give a complete description of particle behaviour.

In this paper, we employ the ERT, PEPT and HSI techniques concurrently to investigate the local velocity field and spatial distribution of coarse mono-sized solid particles conveyed in horizontal turbulent pipe flow under varying solid loadings. A new methodology utilizing the ERT system is developed for local solid velocity measurement which, unlike the common cross-correlation technique, does not rely on inducing a pulse conductivity variation in the system. Additionally, a new high-speed imaging analysis procedure is devised for analysing highly concentrated suspension flows. The accuracy of the local solid velocities and concentration distributions obtained from ERT, PEPT and HSI is systematically assessed on the basis of mass flow continuity and compared. Thus, the performance of these techniques is critically evaluated individually and when coupled in the form of binary hybrids. This study contributes to the advancement of experimental methodologies and analyses pertaining to particle-liquid flows.

2. Experimental

2.1. Pipe flow loop

The pipe flow loop used to study the flow characteristics of turbulent particle-liquid suspensions in a horizontal pipe is schematically represented in Fig. 1. The flow was sustained by a disc pump (Model 2015–8-2HHD, Discflo, USA) through a 5 m long Perspex pipe having an internal diameter $D = 0.04$ m. In-line measurements of the volumetric mixture flowrate were obtained using a Doppler ultrasonic flowmeter (UF D5500, Doppler flow meter, Micronics). The accuracy of the measurements was verified independently at the pipe outlet by bucket and stopwatch measurements, also enabling determination of the average particle delivery concentration. The flow temperature was monitored using a temperature probe. The carrier fluid was water and the dispersed phase consisted of 4 mm mono-sized spherical Nylon-66 particles of density $\rho_p = 1130$ kg m^{-3}. To ensure fully developed flow without any influence from the entrance pipe bend, flow imaging was conducted downstream of a 75D entrance length (i.e., 3 m), as shown in Fig. 1. Four particle volume mean concentrations, i.e., 5, 10, 20 and 26 vol% were examined and the experimental conditions are summarised in Table 1.

Table 1
Experimental conditions.

Particle diameter, d_p (mm)	4
Mean particle concentration, C (vol%)	5, 10, 20, 26
Mean mixture velocity, u_{mean} (m s^{-1})	0.77
Pipe Reynolds number, Re (−)	28,000
Temperature, (°C)	20
Liquid density, ρ_l (kg m^{-3})	998
Particle density, ρ_s (kg m^{-3})	1130

2.2. Electrical resistance tomography

ERT is a soft-field tomographic system in which an electric current is introduced into the examined medium. The resulting distribution of the electric field is contingent upon the intrinsic electrical properties of the material. The instrument typically consists of an ERT sensor, a data acquisition system (DAS), and an ERT imaging reconstruction algorithm, as depicted in Fig. 2. The ERT sensors comprises a 0.04 m diameter pipe section featuring two ring electrodes, each equipped with 16 non-intrusive electrodes positioned equidistantly around the pipe. The electrodes are constructed from stainless steel and the separation between the electrode planes is 0.15 m. Data acquisition is conducted using an ITS p2+ ERT system employing a cross-correlation current injection strategy [29]. The measurement principle underlying the adjacent sensing strategy involves the injection of an excitation current through a pair of adjacent electrodes, as shown in Fig. 2. Subsequently, the potential difference is measured across the remaining pairs of adjacent electrodes until a full rotation is completed, giving a total number of 104 independent differential voltage measurements for a configuration with 16 electrodes. These voltage measurements are then utilized to reconstruct the conductivity distribution across the pipe section using the inbuilt modified sensitivity coefficient back projection algorithm [30,31]. The choice of the reconstruction algorithm involves a compromise between the desired resolution and processing time. Back projection algorithms, owing to their reduced computational time requirements, are usually preferred [32]. Nonetheless, depending on the flow characteristics and experimental objectives, alternative reconstruction algorithms may be considered. The reconstruction of the radial particle concentration and velocity profiles is discussed further below.

2.3. Positron emission particle tracking

As introduced above, PEPT is an advanced non-intrusive technique that employs positron-emitting particle tracers to faithfully track the motion of flow components in 3D space and time, accurately yielding their long-term 3D Lagrangian trajectories. PEPT is now a mature and well-established technique which has been used to investigate various flow phenomena. Comprehensive information about the technique, including details of hardware, software and usage protocols can be found in many of our previous publications [9,33–36]. The resolution of PEPT is comparable to that of PIV and LDV [10,37]. PEPT imaging measurements are conducted using γ-ray detectors over a pipe length of 0.4 m (Fig. 1). The approach typically involves the introduction of a single particle tracer into the pipe loop, enabling it to circulate numerous times to map the entire area of interest. In this study, however, 8 such tracers consisting of 150 μm resin tracers activated with ^{18}F, imbedded inside representative Nylon-66 particles, were used simultaneously to track the solid phase, enhancing data capture rate and

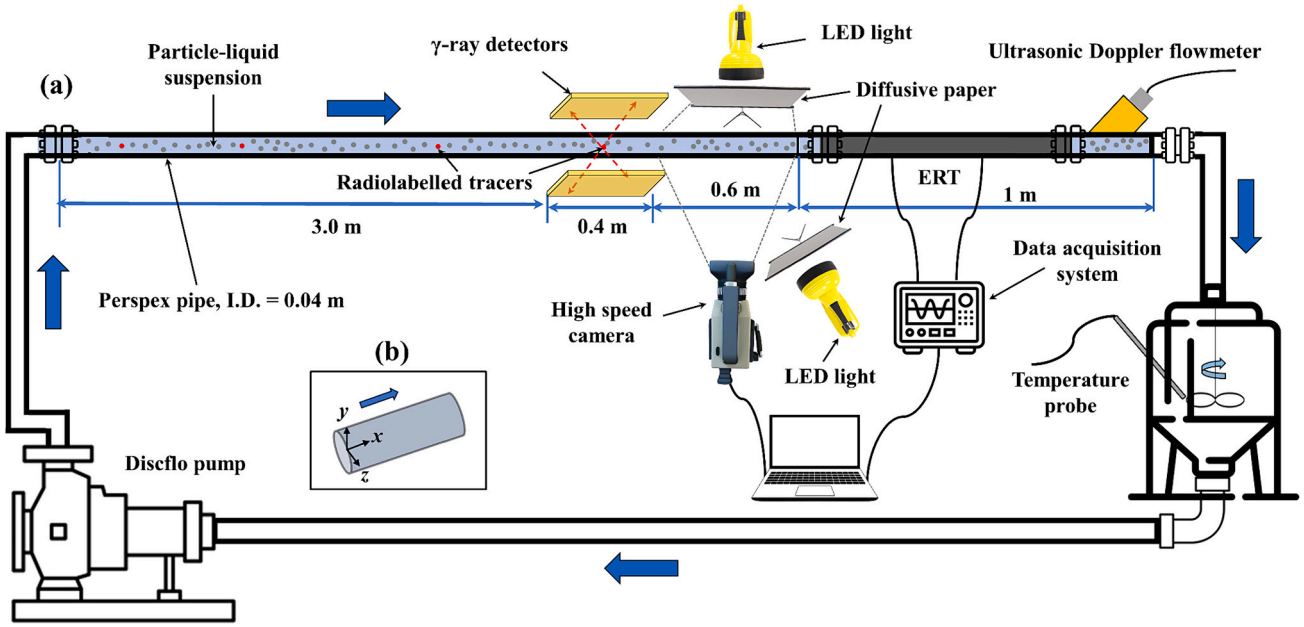

Fig. 1. Experimental set-up: (a) particle-liquid flow loop and flow imaging instrumentation; (b) Cartesian coordinate frame.

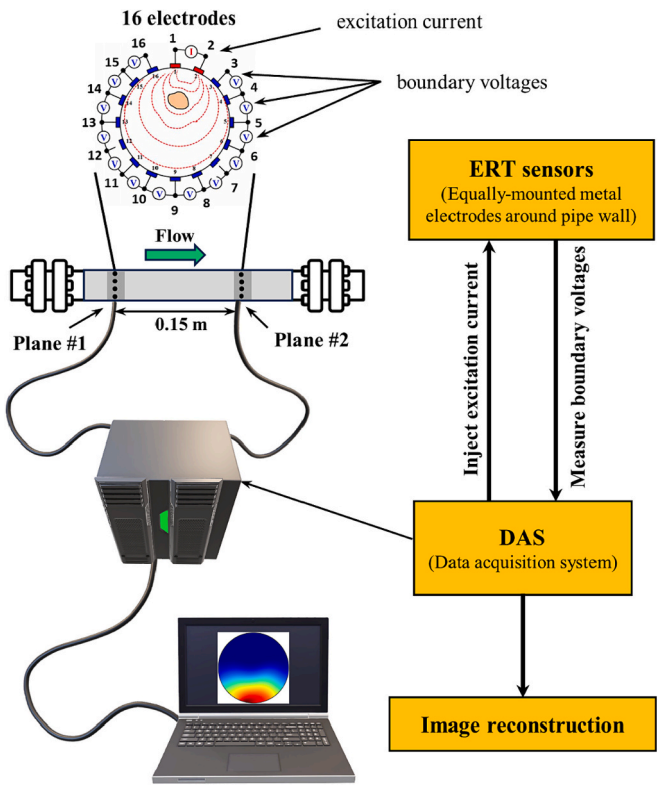

Fig. 2. A 16-electrode dual-plane ERT sensor assembly and data acquisition system.

reducing experimental time.

2.4. High-speed digital imaging

A high-speed digital camera (Photron FASTCAM Mini AX100 540 K M3 model) was utilized to image the particle-liquid flow, as depicted in Fig. 1. The camera was configured to capture the dynamic behaviour of fluid particles at a rate of 4000 frames per second. To enable precise imaging, a standard F-mount lens (Tamron SP Di, AF 90 mm 1:2.8 Nacrp 1:1) was employed featuring a 90 mm focal length and a maximum aperture of f/2.8. High-speed imaging necessitates the deployment of continuous high intensity lighting sources, owing to the exceedingly brief exposure times needed to immobilise the motion of dynamic objects; here, the exposure time was 40 μs. The illumination strategy adopted involved a combination of back- and front-light illumination, employing two lighting instruments (GS Vitec model Multiled LT-v9–15), as shown in Fig. 1. Furthermore, light diffusion paper (Rosco *E*-colour 129, Heavy Frost) was affixed in front of the illumination sources to enhance light diffusion and uniformity.

3. Data analysis

3.1. ERT data analysis

3.1.1. Solid phase distribution

The conductivity distribution across the pipe obtained from the ERT plane sensors is utilized to determine the particle concentration distribution, given the conductivities of the particles and the carrier liquid, based on Maxwell's relationship for particle-liquid flow [38], thus:

$$\alpha_s = \frac{2\sigma_1 + \sigma_2 - 2\sigma_{mc} - \frac{\sigma_{mc}\sigma_2}{\sigma_1}}{2\sigma_1 - 2\sigma_2 + \sigma_{mc} - \frac{\sigma_{mc}\sigma_2}{\sigma_1}} \quad (1)$$

where, α_s represents the particle concentration in each pixel; σ_1, σ_2 are the conductivities of the liquid and particle, respectively, whilst σ_{mc} denotes the ERT-measured mixture conductivity in each pixel of the 316-pixel mesh illustrated in Fig. 3a. This coarse mesh was used solely for conductivity data capture, but to construct the two-phase flow field across the pipe, it was further refined using Spline interpolation to produce a 3 times finer mesh.

The liquid conductivity was determined using a liquid conductivity meter (Jenway 4510), and the particle conductivity was determined using a solid sheet conductivity meter (Ossila Four-point probe). By applying Eq. (1), the particle concentration tomogram was calculated. Subsequently, a row-averaged computation was performed to derive the radial particle concentration profile, as depicted in Fig. 3a. The conductivity data were acquired at a sampling frequency of 100 frames per second for each spatial plane. In each experiment, 3000 images were recorded in each plane to reconstruct the particle distribution in the flow.

3.1.2. Particle velocity field

In the cross-correlation approach for determining the axial velocity distribution of materials, dual images depict the conductivity distribution in the upstream and downstream planes at a specific time, as illustrated in Fig. 3b. The pixel-to-pixel correlation method establishes the relationship between signals from the two planes. By determining the time delay and considering the distance between the planes, the material axial velocity in each pixel can be estimated. However, this method is constrained to pulse changes in conductivity, making it suitable for multiphase flows where the dispersed phase introduces a pulse change (as exemplified in Fig. 3b). Typical conductivity signals obtained from planes #1 and #2 in our particle-liquid pipe flow are displayed in Fig. 4a, which show the absence of any pulse changes. Consequently, the conventional cross-correlation method is not readily applicable and, hence, a different approach is needed to determine the particle velocity field.

Where there are no inherent pulse changes in conductivity, such as in our particle-liquid pipe flow, artificial pulses can be generated by introducing a small sample of a secondary solution with distinct conductivity, such as an electrolyte solution. This method was demonstrated by Sharifi and Young [39] to determine the velocity profile of a single-phase liquid in a horizontal pipe. Whilst, if carefully conducted, such an approach would enable direct measurement of the velocity of the continuous phase, to extract the velocity field of dispersed particles in a particle-liquid flow required the development of more elaborate analysis. The present study determined that the addition of 500 ml of 1 wt% aqueous NaCl solution in 30 kg of primary solution (i.e., water) was optimal to induce the desired pulse change in the conductivity of the primary solution of the particle-liquid flow without significantly affecting the properties of the flow. The resulting conductivity signals at a typical pixel in planes #1 and #2 are depicted in Fig. 4b, showing a clear step change in conductivity which is enlarged in Fig. 4c. At this stage, the cross-correlation approach is called upon to determine the time delay between signal pulses.

In dealing with noisy data resulting from the high conductivity of the experimental medium and the small cross-sectional area of the electrodes, a data filtering strategy is employed. Each measurement frame is replaced by the average of its eight neighbouring frames to mitigate noise and eliminate overlapping issues. As depicted in Fig. 4d, whilst this strategy effectively filters out noise and resolves the issues due to overlapping, it does not cause any temporal shift in the data which could introduce measurement errors. Within the area of focus, the proposed methodology involves comparing the conductivity at a specific pixel in plane #2 to its corresponding delayed conductivity in plane #1. The smallest time delay at which the conductivity in plane #2 reaches that in plane #1 is determined for each measurement frame in the area of focus, as shown in Fig. 4d, i.e., points m_1 and k_1, m_2 and k_2, m_3 and k_3 and so on. The mean of these values is considered the time delay for the given pixel, and the local liquid phase velocity in the pixel is then estimated using

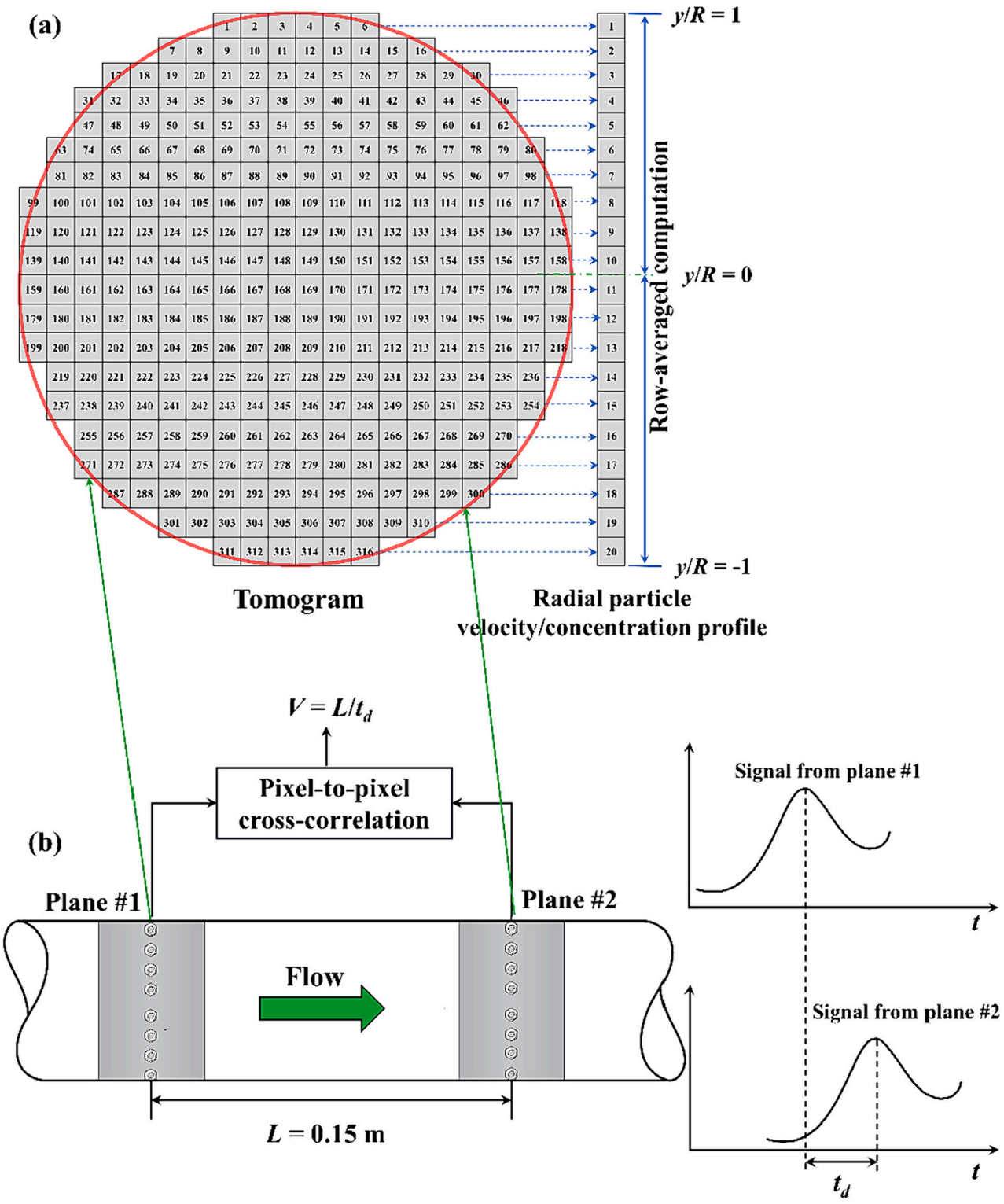

Fig. 3. Flow reconstruction by ERT: (a) 316-pixel mesh for image reconstruction of radial particle concentration profile; (b) principle of conventional cross-correlation for axial velocity measurement.

the known distance between the two planes, set at 15 cm in this experimental setup.

The above procedure provides the liquid phase velocity field in the particle-liquid flow. The particle velocity field can then be inferred using the momentum transfer equation. The momentum transfer equation for the axial velocity of the solid phase ($\boldsymbol{u}_{x,s}$) in a particle-liquid flow can be expressed by considering the balance of forces acting on the solid particles in the axial direction [40], thus:

$$\frac{\partial}{\partial t}\left(\alpha_s \rho_s \boldsymbol{u}_{x,s} A\right) + \frac{\partial}{\partial r}\left(\alpha_s \rho_s \boldsymbol{u}_{x,s}^2 A\right) = \alpha_s \rho_s \boldsymbol{g} A - \frac{\partial}{\partial r}\left(\alpha_s \boldsymbol{\tau}_{ls}\right) + \alpha_s \boldsymbol{S}_s A \tag{2}$$

where, α_s is the volume fraction of the solid phase and ρ_s is its density, A is the cross-sectional area of the pipe, $\boldsymbol{g}$ is the acceleration due to gravity, $\boldsymbol{\tau}_{ls}$ is the shear stress between the liquid and solid phases and $\boldsymbol{S}_s$ is the

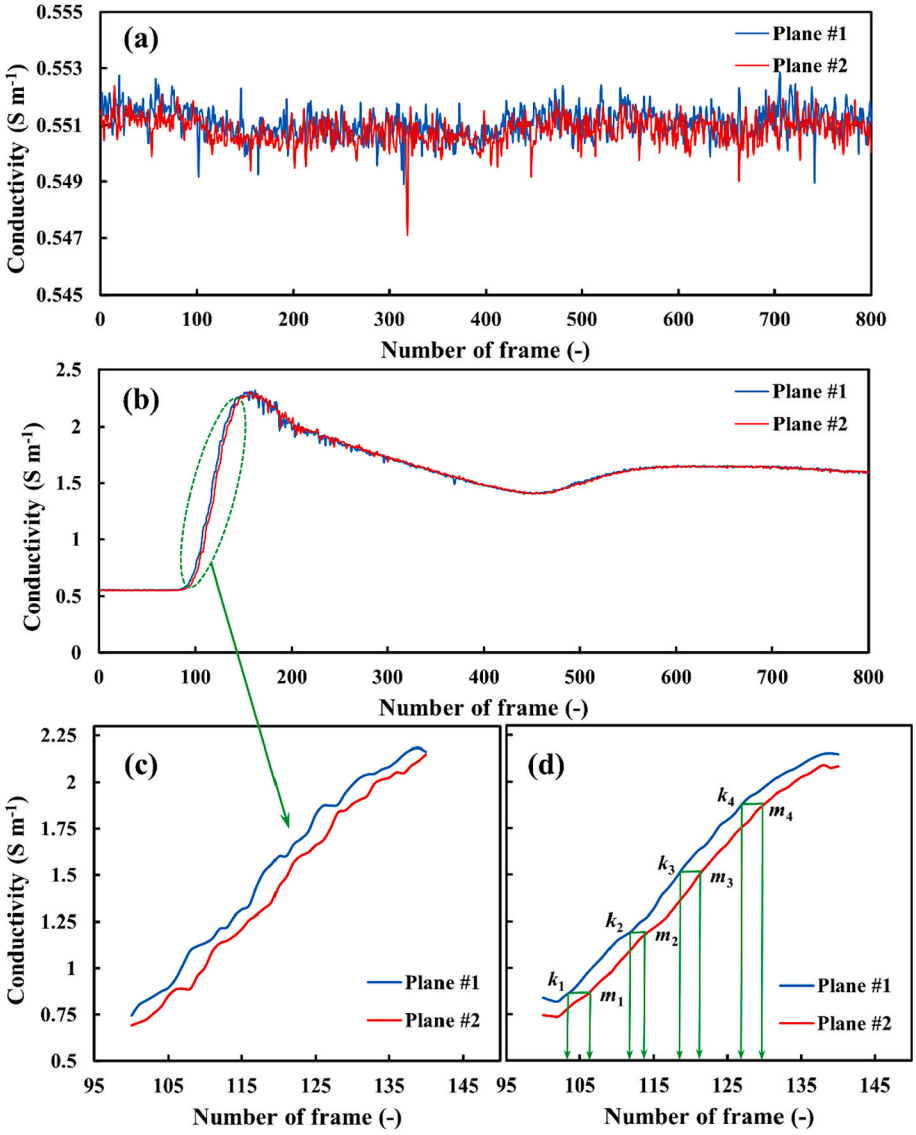

Fig. 4. Typical conductivity signals measured at plane #1 and #2 in particle-liquid flow (C = 5 vol%): (a) without addition of NaCl solution; (b) with addition of NaCl solution; (c) enlarged area of focus; (d) denoised signals in the area of interest.

source term representing any additional forces acting on the solid phase per unit volume. The shear stress ($\boldsymbol{\tau}_{ls}$) between the liquid and solid phases can be expressed using a drag model, such as the Schiller-Naumann equation [41]:

$$\boldsymbol{\tau}_{ls} = \frac{3}{4}\frac{\alpha_s C_d \rho_l |\boldsymbol{u}_{x,l} - \boldsymbol{u}_{s,x}|(\boldsymbol{u}_{x,l} - \boldsymbol{u}_{s,x})}{d_p} \tag{3}$$

where, C_d is the drag coefficient, ρ_l is the density of the liquid phase and $\boldsymbol{u}_{x,l}$ its axial velocity, and d_p is the particle diameter. C_d can be estimated based on the particle Reynolds number (Re_p) using an appropriate correlation such as [41]:

$$C_d = \frac{24}{Re_p}\left(1 + 0.15 Re_p^{0.687}\right) \text{ for } Re_p < 1000 \tag{4}$$

where,

$$Re_p = \frac{\rho_l |u_{x,l} - u_{s,x}| d_p}{\mu_l} \tag{5}$$

where, μ_l is the liquid viscosity. Solving the momentum equation whilst omitting the $\boldsymbol{S}_s$ term and considering steady flow, yields the local axial particle velocity in each pixel within the ERT mesh across the pipe.

3.2. PEPT data analysis

3.2.1. Solid phase distribution

PEPT trajectories enable the spatial distribution of the dispersed particles within the pipe to be also determined. To represent the pipe domain, a 3D grid consisting of equal-volume cells is utilized. Traditionally, the occupancy of a tracer in each cell has been defined as the fraction of the total experimental time (t_∞) spent by the tracer in that specific cell. Such a definition is influenced by the density of the grid, so that as the number of cells increases, the occupancy tends to zero [42]. To circumvent this problem, the concept of ergodic time (t_E) is introduced, assuming a single-phase ergodic system. Ergodic time represents the time a tracer would spend in a cell if it had an equal probability of being present anywhere within the flow. In the case of equal-volume cells, t_E is calculated as the total experimental time divided by the total number of cells, expressed as $t_E = t_\infty / N_c$. To define the local occupancy (O_E), we consider Δt as the time spent by the tracer inside a specific cell, i.e., $O_E = \Delta t / t_E$. Our previous studies showed that the local occupancy defined in this way is equivalent to the ratio of the local solid

volume concentration (c) to the mean volume concentration of solids in the pipe (C) [18,42]. By utilizing these defined quantities, the spatial distribution of the solid phase within the pipe could be accurately estimated.

3.2.2. Particle velocity field

PEPT measurements enable calculation of the instantaneous local velocities of the tracked flow component, in this case the dispersed Nylon-66 particles, by deriving time derivatives from its Lagrangian 3D trajectories. In each experiment, PEPT data were acquired over a two-hour period, yielding approximately 650 particle trajectories. Fig. 5a illustrates typical PEPT particle trajectories at a mean solid concentration of 5 vol%, highlighting distinct particle behaviours in different regions of the pipe. The distribution of PEPT tracer locations across the pipe is depicted in Fig. 5b, from which local Lagrangian velocities can be obtained as follows:

$$\boldsymbol{u} = u_x\boldsymbol{e}_x + u_y\boldsymbol{e}_y + u_z\boldsymbol{e}_z = \frac{dx}{dt}\boldsymbol{e}_x + \frac{dy}{dt}\boldsymbol{e}_y + \frac{dz}{dt}\boldsymbol{e}_z \quad (6)$$

where, t represents time and $\boldsymbol{e}_x$, $\boldsymbol{e}_y$, $\boldsymbol{e}_z$ are, respectively, the unit vectors of the Cartesian x, y, z coordinates. In pipe flow, emphasis is solely placed on the axial velocity component (u_x), as radial motion is considered negligible. The determination of axial velocity involves regression analysis to ascertain the slope of a line fitted to particle tracer positions (x-locations) over time, as shown in Fig. 5c. To ensure the true axial nature of the estimated velocity and minimize the impact of radial fluctuations, ten consecutive x-locations covering a distance <25 mm were utilized. Local particle velocities were subsequently derived using the same mesh used in the ERT calculations (Fig. 3a), thereby facilitating the construction of the radial particle velocity profile.

3.3. HSI data analysis

3.3.1. Image preprocessing

The quality of the captured images is primarily influenced by the lighting conditions, the optical characteristics of the particle surfaces and the imaging hardware. However, digital enhancement procedures were employed to optimise image quality. The initial step in image preprocessing involved adjusting contrast and the application of the Wiener filter for partial noise reduction, a technique used for image restoration and noise reduction, which is designed to improve the quality of images that have been degraded by various types of noise, such as Gaussian noise, motion blur or other forms of distortions. The Wiener filter helps to estimate the original clean image by minimizing the mean squared error between the estimated image and the original image. Due to its inherent low pass filtering attributes, however, such a filter may induce a slight blurring effect on particle edges. Nevertheless, it remains an effective method for mitigating noise-induced degradation in images [43]. The positive effects of contrast adjustment and Wiener filter are demonstrated in Fig. 6, showing clearly a noticeable image enhancement. As a result, such image preprocessing was performed prior to any image processing.

3.3.2. Particle velocity field

The high frame rate (4000 fps) and the high-quality of the images obtained facilitated the development of a particle tracking velocimetry (PTV) algorithm to analyse particle displacement over the short time interval between consecutive frames and, hence, obtain the local particle velocity. In this respect, the accuracy of particle detection assumes a pivotal role in the accurate calculation of the particle velocity field. To enhance particle detection efficiency, the particles used were of two distinct colours, with 70% being blue and 30% white. Typical flow images corresponding to frames #1, #10 and #20 are displayed in Fig. 7, which show that white particles are readily distinguishable from their blue counterparts, highlighting the effectiveness of the adopted colour-coding approach. The white particles are detected using the circle Hough transform to find the circle centre and radius [44], as illustrated in Fig. 7.

The camera sensor is able to digitize the luminance of individual pixels using an 8-bit scale of (monochromatic) grey, where each bit represents an integer value in the range 0 to 255. A zero value indicates a minimally illuminated pixel, rendering it dark when viewed in the image display, and a value of 255 corresponds to maximum illumination,

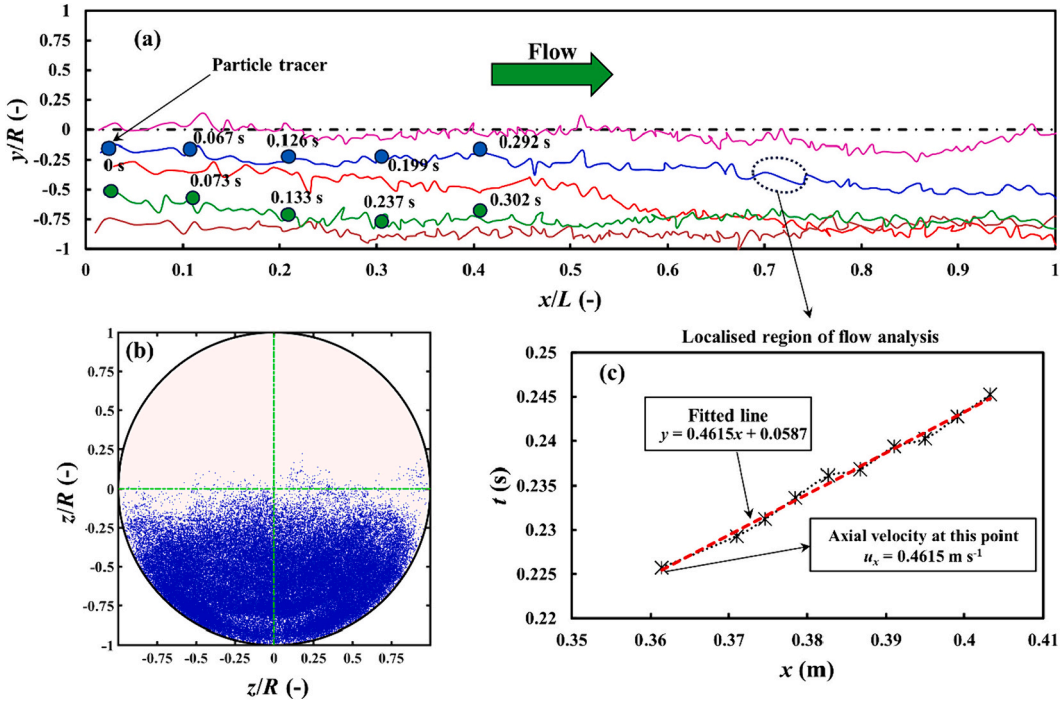

Fig. 5. Illustration of PEPT data analysis (C = 5 vol%): (a) typical particle trajectories; (b) PEPT particle tracer locations acquired over two hours; (c) calculation of local axial particle velocity.

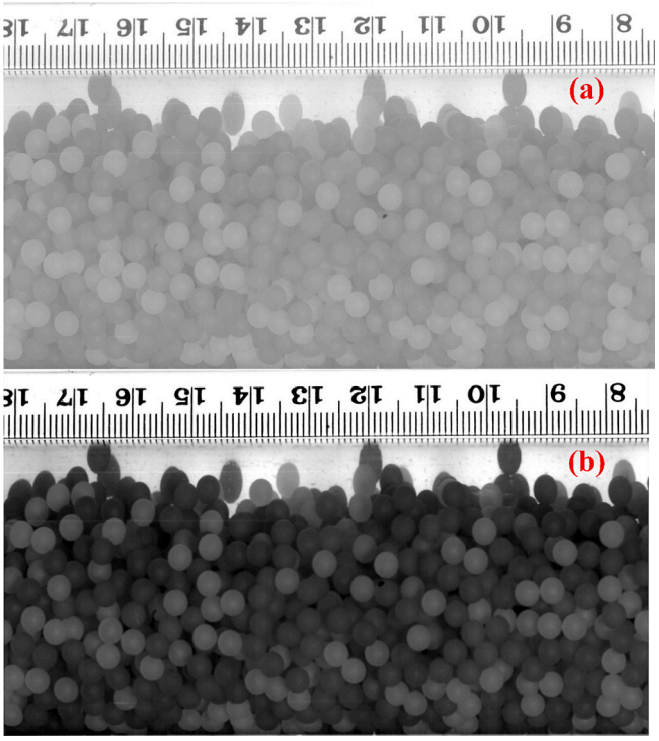

Fig. 6. Typical HSI frame enhanced by preprocessing through contrast adjustment and Wiener filter: (a) before preprocessing; (b) after preprocessing.

making the pixel appear nearly white. Image preprocessing aims to increase the grayscale intensity contrast between the two colours. Conversion of flow images into a binary representation, i.e., image segmentation, was achieved through the implementation of a straightforward auto-thresholding operation involving the following steps:

(a) Computation of the weighted average grey level, denoted as g1.
(b) Computation of weighted average grey levels g2 and g3, spanning the ranges (0, g1) and (g2, 255), respectively.
(c) The threshold value was established as (g2 + g3)/2.

These steps collectively form the foundational framework of the image segmentation process. The segmentation results for two specific frames within the flow (frames #1 and #20 from Fig. 7), are depicted in Fig. 8. Fig. 8a and b showcase the pre-processed images, whilst Figs. 8c-f display the corresponding binary representations obtained after segmentation. It should be noted that the number of particles detected is contingent upon the chosen threshold for image segmentation. However, to analyse a given flow, it is usually sufficient to detect a number of particles that adequately cover the entire cross-section of the pipe, thus, enabling the calculation of local particle velocities in every pixel across the pipe. Once an adequate number of particles have been detected, 74 in this instance, they are tracked, and their velocities determined by pairing the particle images from two sequential video fields. For ease of illustration, frames #1 and #20 are used to magnify particle displacements (see Fig. 8g), though, in actual calculations, two consecutive frames are utilized which exhibit very high similarity given the extremely short time interval between them. Such a high similarity streamlines the process of particle detection and image pairing. Through the analysis of the displacements of detected particle centroids and the time intervals between frames, the local Lagrangian particle velocities are estimated. As pointed out above, in pipe flow the axial velocity component assumes paramount significance, whilst radial motion is inconsequential. As a result, the image analysis will focus exclusively on the examination of local axial particle velocities.

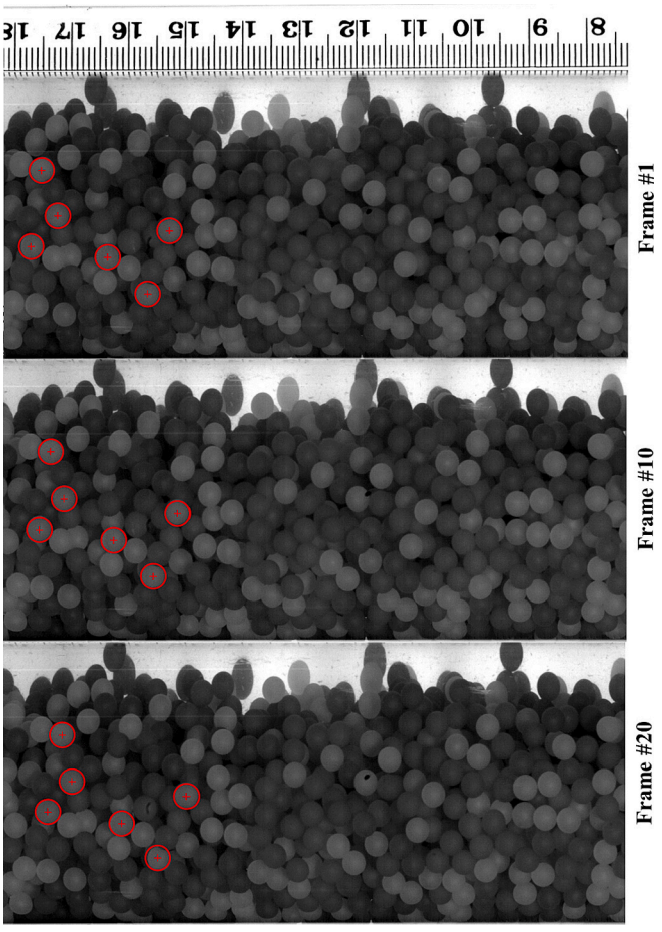

Fig. 7. Typical sequential HSI frames of particle liquid flow: red circles represent examples of white particles detected by the circle Hough transform. (For interpretation of the references to colour in this figure legend, the reader is referred to the web version of this article.)

3.3.3. Solid phase distribution

The solid phase distribution within the pipe can also be obtained from image analysis. Employing a methodology akin to that used for the calculation of local white particle velocities, the total area occupied by white particles can be identified through image segmentation and subsequently transformed into a binary image. The procedure is illustrated in Fig. 9 by considering the binary regions encompassed by white particles in frame #1. By partitioning the cross-sectional area of the pipe into equidistant radial annular bins (20 in this case), the total area covered by the white particles can be quantified. Dividing the total area by the area of a single particle, an estimate of the number of white particles contained in each radial bin is obtained. Now, by considering the proportion of white particles and blue particles within the flow, the radial distribution of the whole solid phase can be evaluated.

4. Results and discussion

This study assesses the capability of three experimental techniques, ERT, PEPT and HSI to examine the velocity field of particles and their spatial distribution in a turbulent particle-liquid pipe flow under different conditions of solid concentration. Results are qualitatively presented in the form of contour plots of local particle velocity and concentration, whilst quantitative evaluation and comparison is facilitated by depicting the radial distributions of local particle velocity and concentration.

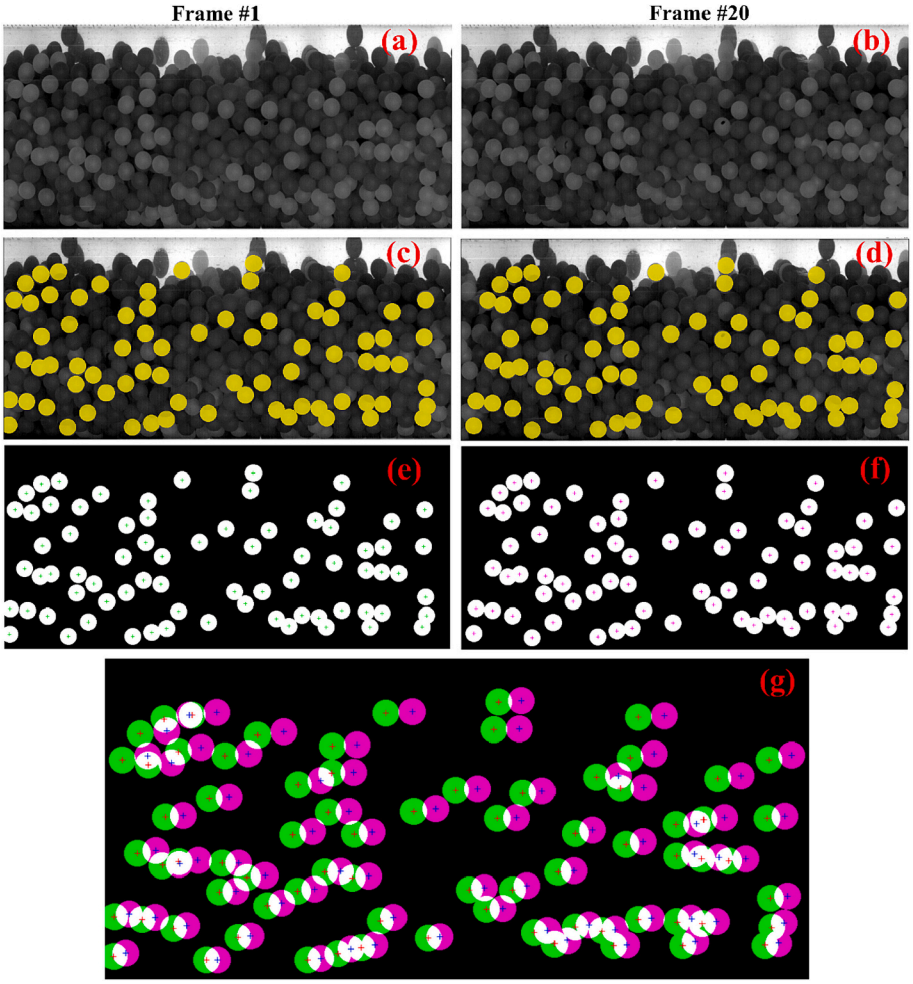

Fig. 8. Sequential HSI images of particle-liquid flow: (a) and (b) raw images; (c) and (d) white particles detected; (e) and (f) binarized images; and (g) white particle displacements between frames #1 and #20.

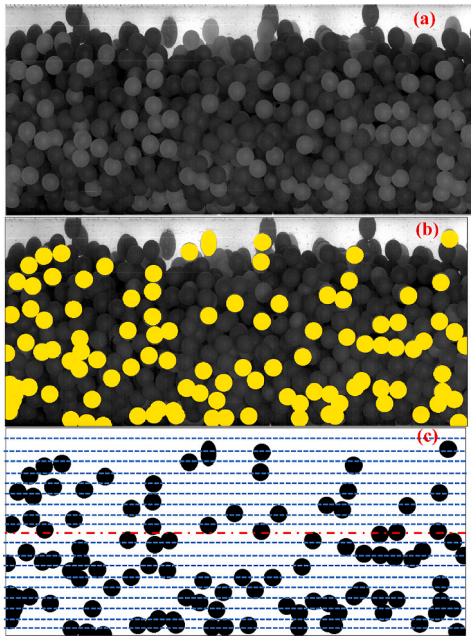

Fig. 9. Typical HSI image used to estimate solid phase distribution: (a) raw image; (b) white particles detected; (c) binarized image with 20 radial bins for evaluating the solid phase distribution.

4.1. Particle bed height

The dynamics of the moving particle bed height assume significant relevance as they influence the flow pattern, pressure gradient and particle distribution within the pipeline. The particle bed height is measured from the bottom of the pipe cross-section to the point where particle concentration reaches zero, averaged over a considerable pipe length (0.4 m). This parameter offers a simple quantitative basis for comparing the three imaging techniques, as shown in Fig. 10. The average particle bed height, as expected, increases as a function of solid loading with particles filling almost the entire pipe cross-section at the highest concentration used, suggesting significant changes in particle dynamics. Notably, there is a good agreement between the measurements obtained from the three techniques, except at the lowest solid fraction of 5%. At lower concentrations, particles exhibit greater mobility leading to increased fluctuations in bed height, but it is difficult to tell a priori which method is more prone to such fluctuations, even though the closer agreement between PEPT and HSI might suggest that it could be ERT.

4.2. Particle velocity field

The contour maps of axial particle velocity normalized by the mean mixture velocity (u_{mean}), measured by PEPT and ERT in the *yz*-plane are displayed in Fig. 11 for various mean solid concentrations. The contour maps were generated using the mesh depicted in Fig. 3a after Spline

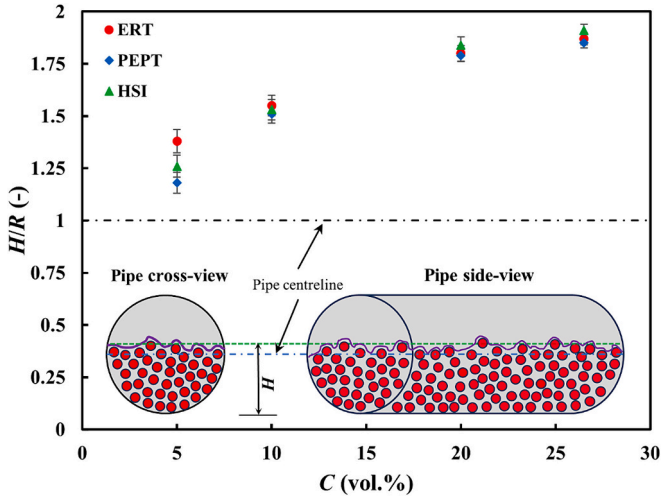

Fig. 10. Average particle bed height as a function of mean solid concentration.

interpolation. The remarkable similarity between the velocity contours generated by the two techniques is noteworthy. Examination of the contour maps reveals distinct patterns in particle movement within the pipe. Particles at the bottom of the pipe are slowest, having velocities 0.6 to $0.9u_{mean}$ over a substantial part of the pipe cross-section. Such a region broadens as the mean solid concentration within the pipe increases, covering approximately half of the pipe cross-section at the highest concentration. Above this region, there is a narrow layer of particles moving at velocities $\sim u_{mean}$. Above this layer, particles are fastest travelling at velocities 1.2 to $1.8u_{mean}$.

The normalized axial particle velocity contour maps superimposed on the axial-radial (u_{rx}) particle velocity vector plots measured by PEPT and HSI in the *xy*-plane are compared in Fig. 12 at different solid loadings, showing a very good agreement. These contour maps corroborate the flow patterns elucidated in Fig. 11 above, with the slowest particles moving within a substantial region at the bottom of the pipe cross-section, underneath a thin layer of particles moving at the mean mixture velocity, and the fastest particles moving above at significantly greater velocities. The axial-radial velocity vectors being principally horizontal, confirm the dominance of axial velocity and negligible stochastic radial motion. The uniform velocity vector field along the pipe also confirms that the flow is fully developed.

A quantitative comparison of ERT, PEPT and HSI is presented in Fig. 13 in the form of radial profiles of normalized axial particle velocity at different mean solid concentrations. The plots show axially-averaged velocity profiles, with the standard deviations displayed as error bars. PEPT has been independently verified for velocity measurements in turbulent flows. We have previously shown that the root mean square (RMS) value of the point differences between two velocity profile curves estimated by PIV and PEPT in a turbulent stirred vessel was <8%, which shows a close agreement between the two techniques [10]. We have also recently shown that turbulent kinetic energy distributions inside a stirred vessel obtained from these two techniques agreed very well [16]. PEPT will, therefore, be taken here as the benchmark for local particle velocity measurements.

For a more quantitative comparison, the standard deviation of the differences observed between PEPT, ERT and HSI were calculated. In each plot where velocity profiles measured by ERT and HSI are compared to a PEPT profile, the RMS value of the point differences between two curves is given in the legend. There is a very good agreement between the HSI and PEPT velocity profiles at low concentrations, which worsens somewhat at higher concentrations. The difference may be attributed to errors caused by the slightly less efficient detection of moving particles at higher solid concentrations by the PTV algorithm as particle overlap increases. Nonetheless, the results show that the HSI technique developed here is very effective at measuring particle velocities even in concentrated flows, circumventing the usual barrier that such opaque flows pose to optical techniques. Similarly, ERT shows a very good agreement at the lowest particle concentration, but the discrepancy with PEPT increases significantly with solid loading, being almost double that of HSI. ERT being an indirect measurement method, relies on a semi-theoretical interpretation of the momentum exchange between the two-phases in the flow which, in addition to the actual conductivity measurements, is also prone to errors. Moreover, increasing the particle concentration leads to more inter-particle interactions which are not considered by the theory. Nevertheless, the enhancements of the ERT method achieved here have enabled the difficult measurement of local particle velocities with reasonable accuracy, which was not possible before.

4.3. Solid phase distribution

The solid phase distributions measured by ERT, PEPT and HSI are presented in Fig. 14 in the form of radial profiles of particle concentration at different mean solid concentrations. ERT is a well-established and proven technique for measuring material distribution [6,7,29,45] and will be taken as the benchmark for measuring local particle concentration. Overall, the concentration profiles exhibit similar trends, showing a very low particle presence in the top part of the pipe cross-section and a substantial accumulation at the bottom, an expected behaviour for dense particles. The uniformity of particle distribution is increasingly enhanced as the solid loading increases. The HSI concentration profiles agree very closely with ERT measurements, except for some minor localised discrepancies. This again demonstrates the effectiveness of the HSI methodology introduced here to analyse concentrated solid-liquid flows.

The main discrepancies are related to the PEPT measurements in the bottom region of the pipe cross-section, and especially at the lower concentrations. As described above, the local particle concentration estimated from PEPT trajectories is based on the assumption that the particle-liquid flow is ergodic. As discussed above in Section 1, such an assumption was shown to hold for the flow of nearly-neutrally buoyant particles [17,18]. However, the differences with respect to ERT observed here seem to suggest that such an assumption may not be entirely valid in the case of denser particles. Ergodicity, in mathematical terms, signifies that a particle tracer, such used in PEPT, within a dynamic or stochastic system will be able to freely visit all regions of the system space in a uniform and random manner and, hence, is able to represent the whole flow. In the flow considered here, particle accumulation at the bottom of the pipe together with the slow-moving particle bed tend to inhibit the free movement of the tracer, thereby affecting the ergodicity of the flow and resulting in inaccurate occupancy calculations. This interpretation is consistent with the low discrepancies in the upper region of the pipe cross-section where particle concentration is low and the tracer is able to move more freely, and the higher differences observed in the lower region of the flow where particle concentration is high and particle velocities are low.

4.4. Mass continuity

In a steady multiphase flow, the volumetric flowrate (Q_c) of a given phase *c* can be calculated from the integral of the product of the local phase velocity of the phase (u_c) and its local volume fraction α_c across the flow, thus:

$$Q_c = \int_A u_c \alpha_c dA \tag{7}$$

where, *A* represents the cross-sectional area of the flow. For a particle-liquid flow, if the distributions of local particle fraction and velocity are known, the solid volumetric flowrate ($Q_{s,est}$) can be estimated using a

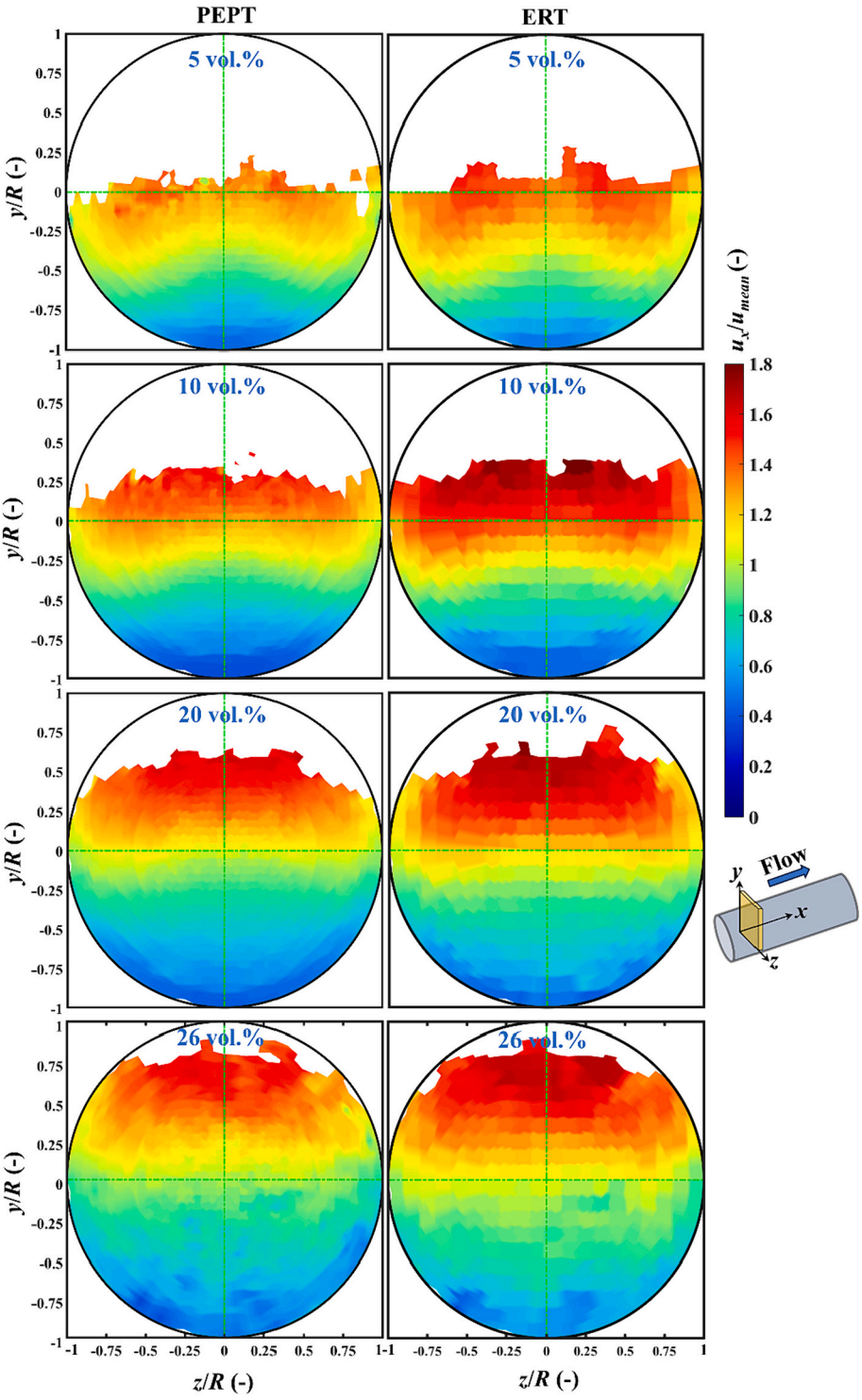

Fig. 11. Contour maps of axial particle velocity in *yz*-plane measured by PEPT and ERT at different mean solid concentrations.

mesh such as the one in Fig. 3a, thus:

$$Q_{s,est} = \sum_{i=1}^{n} u_{x,s,i}\alpha_{s,i}A_i \tag{8}$$

where, $u_{x,s,i}$ and $\alpha_{s,i}$ are, respectively, the local average particle velocity and volume fraction in the i-th pixel of the mesh with area A_i. Since all three techniques (ERT, PEPT, HSI) furnish measurements of both these quantities, the solid volumetric flowrate can be obtained for each one of them. These values can then be compared to the mean solid flowrate measured by the bucket and stopwatch method and the error estimated.

The error is plotted in Fig. 15 as a function of mean solid concentration. Overall, the errors for all three techniques are small (< 9%) and similar, falling within a narrow range 6–8.5%. Nonetheless, significant improvements can be achieved by coupling these techniques in the form of even more efficient hybrids, as shown in Fig. 15. The results indicate that a HSI-ERT hybrid measurement combining velocity estimation from HSI and solid phase distribution from ERT produces significantly smaller errors. On the other hand, a PEPT-ERT hybrid measurement including velocity estimation from PEPT and solid phase distribution from ERT

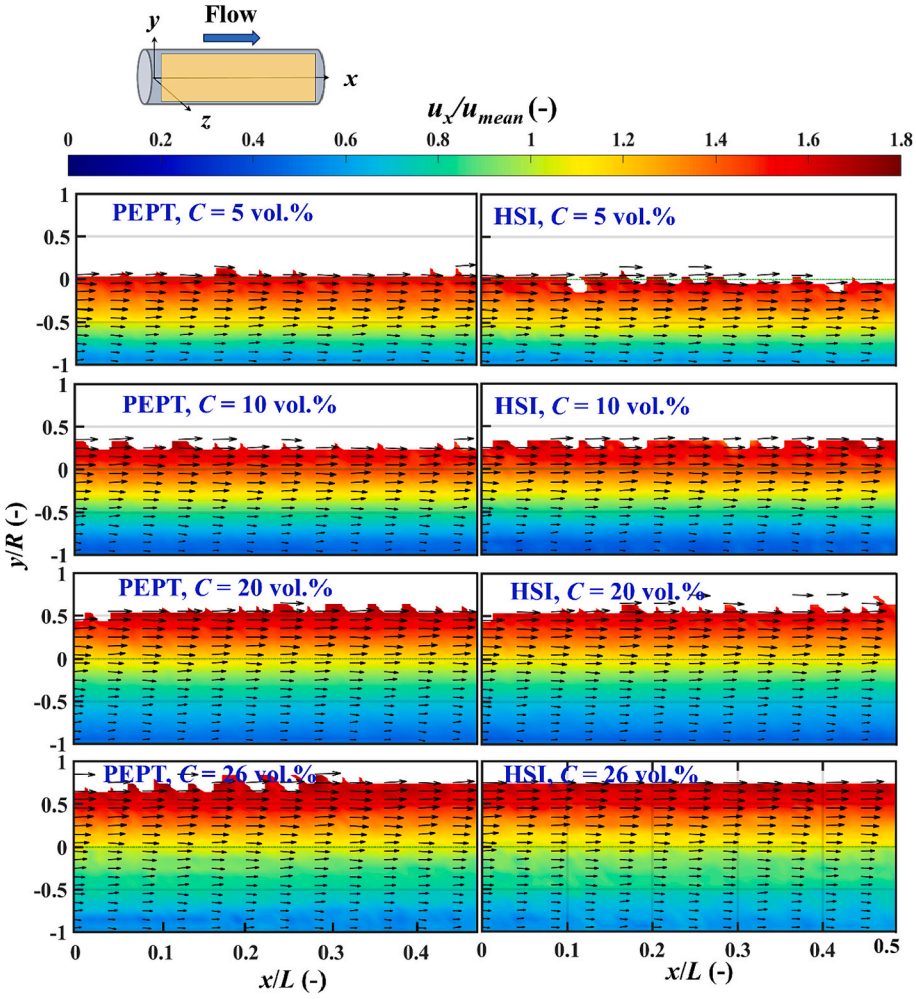

Fig. 12. Axial particle velocity maps measured by PEPT and HSI in *xy*-plane superimposed on axial-radial particle velocity vector maps at different mean solid concentrations.

yields the lowest errors. This corroborates the above stipulation that the velocity estimation from PEPT data and solid phase distribution from ERT provide the most reliable measurements.

5. Conclusion

The study compared three experimental techniques ERT, PEPT and HSI for measuring local particle velocity and spatial particle distribution in a horizontal particle-liquid pipe flow. The new ERT methodology estimated particle velocity without relying on pulse conductivity changes, overcoming limitations of the traditional cross-correlation approach. The enhanced HSI technique was systematically compared with PEPT and ERT at various solid concentrations. PEPT provided the most accurate velocity profiles, followed by HSI, whilst ERT offered the most accurate concentration profiles followed by HSI even at high solid concentrations. All three techniques verified the mass continuity within a small error of <9%. The enhanced HSI has emerged as a simple cost-effective option for complex flow analysis compared to PEPT and ERT which require much more complex protocols. Combining PEPT for local velocity measurement and ERT for particle concentration measurement gave the best comprehensive characterization of the two-phase flow field, demonstrating potential synergies between these methods for complex flow studies. This study contributes to the understanding of particle-laden flows and the selection and development of advanced experimental measurement methodologies for their analysis.

Nomenclature

Symbols

A_i	area of the *i*-th pixel
C	volumetric mean solid concentration, vol%
c	local particle concentration, vol%
D	pipe diameter, m
d_p	particle diameter, m
$\boldsymbol{e}_x$, $\boldsymbol{e}_y$, $\boldsymbol{e}_z$	unit vectors in *x*, *y* and *z* direction
L	pipe axial length, m
n	number of data points
Q_c	volumetric flowrate of phase c, $m^3\ s^{-1}$
Q_s	true volumetric solid flowrate, $m^3\ s^{-1}$
$Q_{s,est}$	estimated volumetric solid flowrate, $m^3\ s^{-1}$
r	radial position, m
R	pipe radius, m
Re	pipe Reynolds number
Re	particle Reynolds number
RMS	root mean square
t	time, s
u	local velocity, $m\ s^{-1}$
u_{mean}	mean mixture velocity, $m\ s^{-1}$
x	*x*-direction position, m
y	*y*-direction position, m
z	*z*-direction position, m

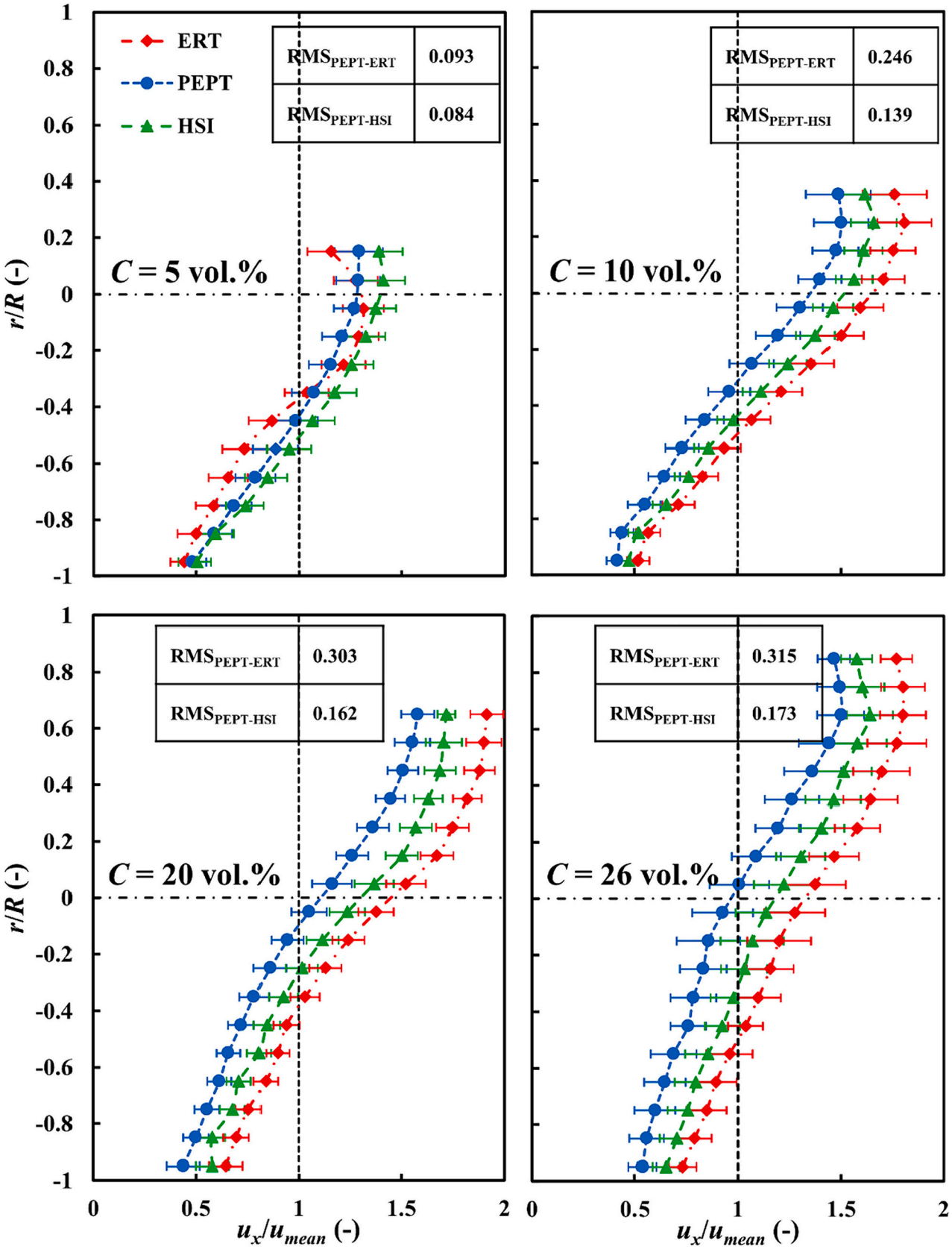

Fig. 13. Radial profiles of axial particle velocity at different mean solid concentrations.

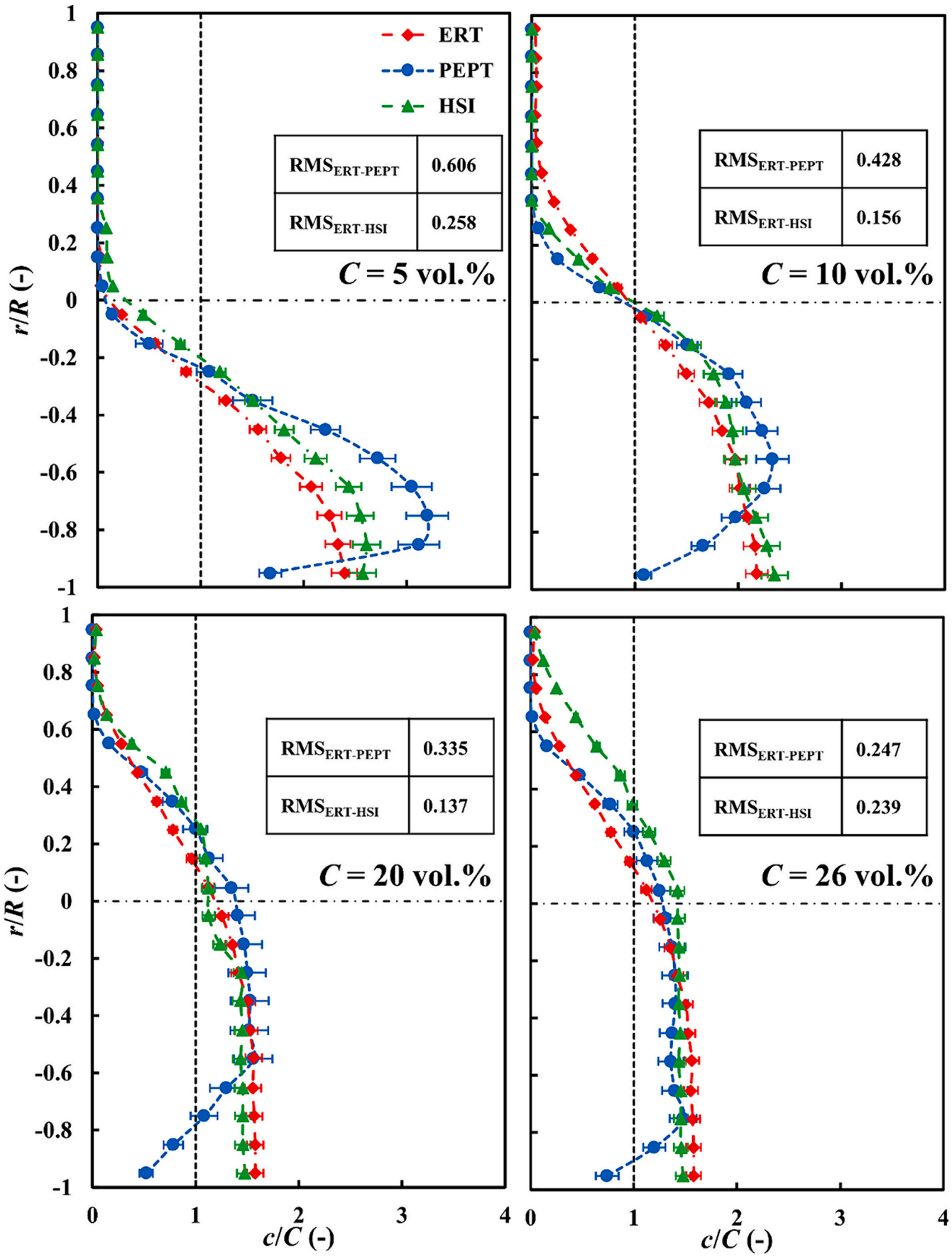

Fig. 14. Radial distributions of particles at different mean solid concentrations.

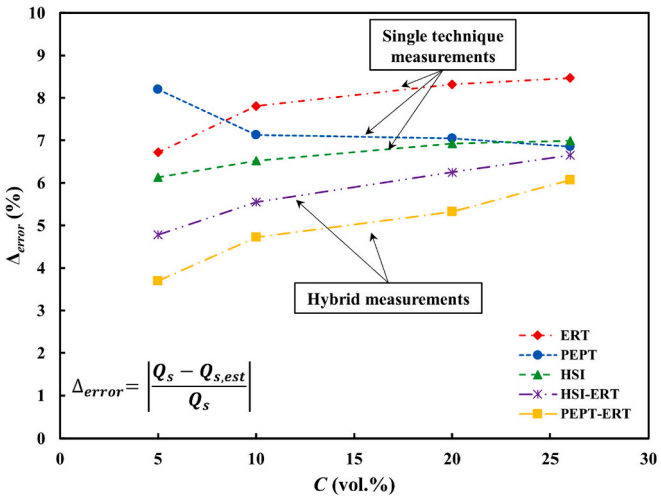

Fig. 15. Error of volumetric solid flowrate estimated from individual PEPT, ERT and HSI techniques and their hybrids.

Greek symbols

α_s	volume fraction
Δ_{error}	error of volumetric solid flowrate ($\left\|\frac{Q_s-Q_{s,est}}{Q_s}\right\|$)
σ_1	liquid electrical conductivity, S m^{-1}
σ_2	particle electrical conductivity, S m^{-1}
σ_{mc}	mixture electrical conductivity, S m^{-1}
μ_l	liquid viscosity, kg m^{-1} s^{-1}
ρ_l	liquid density, kg m^{-3}
ρ_s	particle density, kg m^{-3}

Abbreviations

ERT	Electrical Resistance Tomography
HSI	High-Speed Imaging
LDA	Laser Doppler Anemometry
PEPT	Positron Emission Particle Tracking
PIV	Particle Image Velocimetry
PTV	Particle Tracking Velocimetry

CRediT authorship contribution statement

Chiya Savari: Writing – original draft, Visualization, Validation, Software, Methodology, Investigation, Formal analysis, Conceptualization. **Kun Li:** Visualization, Validation, Software, Methodology, Investigation, Formal analysis, Conceptualization. **Mostafa Barigou:** Writing – review & editing, Validation, Supervision, Resources, Project administration, Methodology, Funding acquisition, Conceptualization.

Declaration of competing interest

The authors declare that they have no known competing financial interests or personal relationships that could have appeared to influence the work reported in this paper.

Data availability

The data that support the findings of this study are available within the article

Acknowledgement

This work was supported by EPSRC Programme Grant EP/R045046/1: Probing Multiscale Complex Multiphase Flows with Positrons for Engineering and Biomedical Applications (PI: Prof. M. Barigou, University of Birmingham).

References

[1] M. Parsi, K. Najmi, F. Najafifard, S. Hassani, B.S. McLaury, S.A. Shirazi, A comprehensive review of solid particle erosion modeling for oil and gas wells and pipelines applications, J. Nat. Gas Sci. Eng. 21 (2014) 850–873.
[2] Z. Yang, X. Lian, C. Savari, M. Barigou, Evaluating the effectiveness of CFD-DEM and SPH-DEM for complex pipe flow simulations with and without particles, Chem. Eng. Sci. 288 (2024) 119788.
[3] G. Lucas, J. Cory, R. Waterfall, W. Loh, F. Dickin, Measurement of the solids volume fraction and velocity distributions in solids–liquid flows using dual-plane electrical resistance tomography, Flow Meas. Instrum. 10 (1999) 249–258.
[4] Y. Ma, Z. Zheng, L.-A. Xu, X. Liu, Y. Wu, Application of electrical resistance tomography system to monitor gas/liquid two-phase flow in a horizontal pipe, Flow Meas. Instrum. 12 (2001) 259–265.
[5] W. Loh, R. Waterfall, J. Cory, G. Lucas, Using ERT for multi-phase flow monitoring, in: 1st World Congress on Industrial Process Tomography, Buxton, Greater Manchester, 1999, pp. 47–53.
[6] M. Wang, G. Lucas, Y. Dai, N. Panayotopoulos, R.A. Williams, Visualisation of bubbly velocity distribution in a swirling flow using electrical resistance tomography, Part. Part. Syst. Charact. 23 (2006) 321–329.
[7] S. Razzak, S. Barghi, J. Zhu, Measurement of holdup and propagation velocities in a liquid-solid circulating fluidized bed using electrical resistance tomography, in: 2007 AIChE Annual Meeting, 2007.
[8] S. Razzak, S. Barghi, J.-X. Zhu, Y. Mi, Phase holdup measurement in a gas–liquid–solid circulating fluidized bed (GLSCFB) riser using electrical resistance tomography and optical fibre probe, Chem. Eng. J. 147 (2009) 210–218.
[9] M. Barigou, Particle tracking in opaque mixing systems: an overview of the capabilities of PET and PEPT, Chem. Eng. Res. Des. 82 (2004) 1258–1267.
[10] P. Pianko-Oprych, A. Nienow, M. Barigou, Positron emission particle tracking (PEPT) compared to particle image velocimetry (PIV) for studying the flow generated by a pitched-blade turbine in single phase and multi-phase systems, Chem. Eng. Sci. 64 (2009) 4955–4968.
[11] K. Li, C. Savari, H.A. Sheikh, M. Barigou, A data-driven machine learning framework for modeling of turbulent mixing flows, Phys. Fluids 35 (2023).
[12] C. Savari, H.A. Sheikh, M. Barigou, Lagrangian recurrence tracking: a novel approach for description of mixing in liquid and particle–liquid flows, Ind. Eng. Chem. Res. 60 (2021) 18501–18512.
[13] C. Savari, M. Barigou, Lagrangian wavelet analysis of turbulence modulation in particle–liquid mixing flows, Phys. Fluids 34 (2022).
[14] H.A. Sheikh, C. Savari, M. Barigou, Lagrangian stochastic modelling of liquid flow in a mechanically agitated vessel, Chem. Eng. Sci. 249 (2022) 117318.
[15] K. Li, C. Savari, M. Barigou, Computation of Lagrangian coherent structures from experimental fluid trajectory measurements in a mechanically agitated vessel, Chem. Eng. Sci. 254 (2022) 117598.
[16] C. Savari, K. Li, M. Barigou, Multiscale wavelet analysis of 3D Lagrangian trajectories in a mechanically agitated vessel, Chem. Eng. Sci. 260 (2022) 117844.
[17] X. Lian, C. Savari, K. Li, M. Barigou, Coupled smoothed particle hydrodynamics and discrete element method for simulating coarse food particles in a non-Newtonian conveying fluid, Phys. Fluids 35 (2023).
[18] Z. Yang, C. Savari, M. Barigou, Numerical and experimental investigations of horizontal turbulent particle–liquid pipe flow, Ind. Eng. Chem. Res. 61 (2022) 12040–12051.
[19] W. Liang, A. Goharzadeh, P. Rodgers, Experimental Characterization of Hydraulic Solid Particle Transportation in Horizontal Pipelines Using PIV, Fluids Engineering Division Summer Meeting, 2010, pp. 2759–2765.
[20] X. Pan, R. Luo, X. Yang, H. Yang, Three-dimensional particle image tracking for dilute particle-liquid flows in a pipe, Meas. Sci. Technol. 13 (2002) 1206.
[21] R. Shokri, S. Ghaemi, D. Nobes, R. Sanders, Investigation of particle-laden turbulent pipe flow at high-Reynolds-number using particle image/tracking velocimetry (PIV/PTV), Int. J. Multiphase Flow 89 (2017) 136–149.
[22] X. Fu, G. Wang, Z. Dong, Theoretical analysis and numerical computation of dilute solid/liquid two-phase pipe flow, Sci. China, Ser. E Technol. Sci. 44 (2001) 298–308.
[23] S.E. Mena, J.S. Curtis, Experimental data for solid–liquid flows at intermediate and high stokes numbers, J. Fluid Mech. 883 (2020) A24.
[24] N. La Forgia, E.H. Herø, H.A. Jakobsen, High-speed image processing of fluid particle breakage in turbulent flow, Chem. Eng. Sci. X 12 (2021) 100117.
[25] R.G. Morgan, C.N. Markides, I. Zadrazil, G.F. Hewitt, Characteristics of horizontal liquid–liquid flows in a circular pipe using simultaneous high-speed laser-induced fluorescence and particle velocimetry, Int. J. Multiphase Flow 49 (2013) 99–118.
[26] F. Shaffer, B. Gopalan, R.W. Breault, R. Cocco, S.R. Karri, R. Hays, T. Knowlton, High speed imaging of particle flow fields in CFB risers, Powder Technol. 242 (2013) 86–99.
[27] C.E. Willert, High-speed particle image velocimetry for the efficient measurement of turbulence statistics, Exp. Fluids 56 (2015) 1–17.
[28] A.M. Dehkordi, C. Savari, Effects of contaminants on the mass-transfer characteristics of a two-impinging-streams gas-liquid reactor, Chem. Eng. Technol. 34 (2011) 1797–1806.
[29] M. Wang, Q. Wang, B. Karki, Arts of electrical impedance tomographic sensing, Philos. Trans. R. Soc. A Math. Phys. Eng. Sci. 374 (2016) 20150329.

[30] R. Giguère, L. Fradette, D. Mignon, P.A. Tanguy, ERT algorithms for quantitative concentration measurement of multiphase flows, Chem. Eng. J. 141 (2008) 305–317.
[31] C. Kotre, A sensitivity coefficient method for the reconstruction of electrical impedance tomograms, Clin. Phys. Physiol. Meas. 10 (1989) 275.
[32] D.M. Scott, H. McCann, Process Imaging for Automatic Control, CRC Press, 2018.
[33] K. Li, C. Savari, M. Barigou, Predicting complex multicomponent particle–liquid flow in a mechanically agitated vessel via machine learning, Phys. Fluids 35 (2023).
[34] H.A. Sheikh, C. Savari, M. Barigou, A data-driven stochastic model for velocity field and phase distribution in stirred particle-liquid suspensions, Powder Technol. 411 (2022) 117940.
[35] A. Guida, A.W. Nienow, M. Barigou, Mixing of dense binary suspensions: multi-component hydrodynamics and spatial phase distribution by PEPT, AICHE J. 57 (2011) 2302–2315.
[36] Y.S. Fangary, M. Barigou, J.P. Seville, D.J. Parker, A Langrangian study of solids suspension in a stirred vessel by positron emission particle tracking (PEPT), Chem. Eng. Technol. 25 (2002) 521–528.
[37] M. Barigou, F. Chiti, P. Pianko-Oprych, A. Guida, L. Adams, X. Fan, D.J. Parker, A. W. Nienow, Using positron emission particle tracking (PEPT) to study mixing in stirred vessels: validation and tackling unsolved problems in opaque systems, J. Chem. Eng. Jpn 42 (2009) 839–846.
[38] M. Wang, T. Jones, R.A. Williams, Visualization of asymmetric solids distribution in horizontal swirling flows using electrical resistance tomography, Chem. Eng. Res. Des. 81 (2003) 854–861.
[39] M. Sharifi, B. Young, Electrical resistance tomography (ERT) for flow and velocity profile measurement of a single phase liquid in a horizontal pipe, Chem. Eng. Res. Des. 91 (2013) 1235–1244.
[40] T.N. Ofei, A.Y. Ismail, Eulerian-Eulerian simulation of particle-liquid slurry flow in horizontal pipe, J. Petrol. Eng. 2016 (2016).
[41] R. Silva, C. Cotas, F. Garcia, P. Faia, M. Rasteiro, Particle distribution studies in highly concentrated solid-liquid flows in pipe using the mixture model, Procedia Eng. 102 (2015) 1016–1025.
[42] A. Guida, A.W. Nienow, M. Barigou, PEPT measurements of solid–liquid flow field and spatial phase distribution in concentrated monodisperse stirred suspensions, Chem. Eng. Sci. 65 (2010) 1905–1914.
[43] A. Khireddine, K. Benmahammed, W. Puech, Digital image restoration by Wiener filter in 2D case, Adv. Eng. Softw. 38 (2007) 513–516.
[44] T.J. Atherton, D.J. Kerbyson, Size invariant circle detection, Image Vis. Comput. 17 (1999) 795–803.
[45] S. Razzak, S. Barghi, J.-X. Zhu, Application of electrical resistance tomography on liquid–solid two-phase flow characterization in an LSCFB riser, Chem. Eng. Sci. 64 (2009) 2851–2858.